Journal of Luminescence 134 (2013) 113–125

Contents lists available at SciVerse ScienceDirect

Journal of Luminescence

journal homepage: www.elsevier.com/locate/jlumin

Luminescence of $Li_6Gd(BO_3)_3$ crystals upon ultraviolet and inner-shell excitations

I.N. Ogorodnikov *, V.A. Pustovarov

Experimental Physics Department, Ural Federal University, Mira Street, 19, Ekaterinburg 620002, Russia

ARTICLE INFO

Article history:
Received 5 June 2012
Received in revised form
30 August 2012
Accepted 5 September 2012
Available online 15 September 2012

Keywords:
Optical crystal
Lithium–gadolinium orthoborate
$Li_6Gd(BO_3)_3$
Lanthanide ions
Absolute energy locations
Luminescence spectra

ABSTRACT

The paper presents the results of the study on luminescence and electronic excitations in $Li_6Gd(BO_3)_3$ single crystals. The optical and luminescence spectroscopy with a sub-nanosecond time resolution upon selective photoexcitation in the energy range from 3.0 to 650 eV was used to investigate in detail the luminescence of both the Gd^{3+} host ions and Ce^{3+} impurity ions as well as the processes of energy transfer between them. The intrinsic ultraviolet emission at 3.95–3.97 eV due to $^6P_j \rightarrow {}^8S_{7/2}$ transitions in the Gd^{3+} host ion and the fast luminescence at 2.8–3.0 eV due to $5d \rightarrow 4f^1$ dipole-allowed transitions in the Ce^{3+} impurity ion were studied upon excitations through the intracenter, charge transfer, band-to-band, and inner-shell transitions. The specificity of the energy transfer upon excitation of photoluminescence in the energy range of absorption of the inner shells of different atoms of the crystal, as well as in the energy region of the giant resonance of 4d–4f transitions was revealed. On the basis of the experimental data, the bandgap $E_g = 9.3$ eV, the minimum energy of the $5d \rightarrow 4f^1$ and charge transfer transitions were determined. The expected positions of the ground states of the $4f^n$ and $4f^{n-1}5d$ levels of trivalent lanthanide ions as well as the $4f^{n+1}$ and $4f^n5d$ levels of divalent ions were calculated for all the lanthanide ions in $Li_6Gd(BO_3)_3$ host crystal.

1. Introduction

Lithium–gadolinium orthoborate $Li_6Gd(BO_3)_3$ (LGBO) crystals are promising transparent insulators in the vacuum ultraviolet (VUV) region due to their large bandgap (ca. 9 eV [1]). LGBO has the following unique advantages: its intrinsic ultraviolet (UV) luminescence occurs due to the f–f transitions in Gd^{3+} host ions and the emission intensity is not subject to a concentration quenching; LGBO lattice provides a large isomorphous capacity for trivalent rare-earth impurities, which substitute gadolinium host ion in a regular position; one-dimensional chains of gadolinium ions are an efficient channel of energy transfer from the host lattice to the impurity ions [2,3]. Both the intrinsic emission and luminescence of Ce^{3+} and Eu^{3+} impurity ions in LGBO were previously studied at various temperatures ranged from 1.5 to 500 K upon excitation with UV-photons [2–4], VUV-radiation [1], and X-rays [5]. Several research works were devoted to study of LGBO crystals in respect of macro- and micro-defects in as-grown crystals [6], radiation induced defects [7], and short-living defects that are responsible for transient optical absorption [8].

LGBO chemical composition comprises elements that have stable isotopes with large thermal neutron capture cross-sections. ^{10}B and ^6Li are the most important isotopes that provide ca. 2.8 MeV energy at neutron capture. Because of this, LGBO has a great potential in neutron imaging. Czirr et al. [9] reported on the development of a promising thermal neutron scintillator on the basis of LGBO:Ce that can be optimized for specific purposes, in particular, for the exothermic neutron detection. The Ce^{3+} rare-earth ions are widely used as an optically active dopant in modern scintillation detectors and converters of ionizing radiation based on inorganic optical crystals. The impurity Ce^{3+} ion in optical crystals is known as a very efficient recombination center. The final stage of the electron–hole recombination is a dipole-allowed d–f radiative transition in Ce^{3+} ion, registered usually as a fast-decaying (17–60 ns) scintillation signal [10].

In this paper we focus our attention on LGBO crystals doped with Ce^{3+} impurity ions (LGBO:Ce). The main goal of this work is to analyze the relaxation of electronic excitations in LGBO:Ce crystals using optical and luminescence spectroscopy with sub-nanosecond time resolution upon selective photoexcitation in the wide energy range from UV to extreme UV (XUV) energy regions in order to characterize the excitation mechanisms and the energy transfer processes. The main idea of this research work is to obtain the most comprehensive set of spectroscopic data on LGBO and on the basis of these data to determine the electronic structure parameters, such as the bandgap, minimal energy of the

* Corresponding author. Tel.: +7 343 3754711; fax: +7 343 3743884.
E-mail addresses: i.n.ogorodnikov@gmail.com, igor.ogorodnikov@bk.ru, ogo@dpt.ustu.ru (I.N. Ogorodnikov).

0022-2313/$ - see front matter © 2012 Elsevier B.V. All rights reserved.
http://dx.doi.org/10.1016/j.jlumin.2012.09.002

d–f and charge transfer transitions, the ground state locations of the 4f and 5d energy levels of divalent and trivalent lanthanide ions in the LGBO host lattice.

2. Experimental details

The examined LGBO crystals doped with the 0.5 and 4.5 mol% Ce^{3+} ions were grown at the STC Institute for Single Crystals NAS of Ukraine (Kharkov, Ukraine) utilizing the Czochralski technique. The growth process and the lattice parameters of crystals were described in Ref. [11]. The sizes of the investigated crystals were $10 \times 5 \times 2$ mm^3; the largest surfaces studied were polished and parallel. In all cases, the designation LGBO:Ce means the concentration of 4.5 mol% Ce^{3+}. In certain cases, the impurity concentration of Ce^{3+} ions was explicitly specified in parentheses: LGBO:Ce (0.5%) or LGBO:Ce (4.5%).

The present study was carried out by the means of the low-temperature luminescence VUV and XUV spectroscopy with the time resolution. Photoluminescence (PL) spectra in the energy range of 1.2–6.2 eV, PL excitation (PLE) spectra in the energy range 3.7–24 eV (0.32 nm resolution) were measured at 8 and 293 K at the SUPERLUMI experimental station of HASYLAB [12] using synchrotron radiation (SR). Samples were mounted in a sample holder attached to a He-flow cryostat with vacuum not less than 7×10^{-10} Torr. At the storage ring DORIS the full width at half maximum (FWHM) of SR pulses was 130 ps with the repetition period of 192 ns. Such pulses excitation enables the recording of spectra within a time-window correlated with the arrival of SR pulses. In the present experiments we recorded time-resolved spectra within two independent time-windows (TWs) set for detection of luminescence signal within 0.8–18.1 ns (TW1) and 126.8–189.4 ns (TW2) relative to the beginning of the SR pulse. Time-integrated (TI) spectra were recorded within the full time range available between two sequential excitation pulses, viz. 192 ns. The PLE spectra were corrected to an equal number of photons incident on the sample using sodium salicylate. Simultaneously with the excitation, the reflection spectra were recorded at an angle of incidence 17.5°. The 0.3 m ARC Spectra Pro-308i spectrometer equipped either with an R6358P (Hamamatsu) photomultiplier or a CCD camera, which were used as detectors. The PL emission spectra were not corrected to the spectral sensitivity of the recording system.

The time-integrated and time-resolved spectra of PL emission (2.5–8.0 eV) and PL excitation (50–220 eV and 500–650 eV) as well as the PL decay kinetics have been measured at 6 K using SR from the BW3 beamline. The SR from the undulator was further monochromatized by a Zeiss SX700 monochromator. The typical spectral resolution of this monochromator was 50 and 900 meV in the energy regions around *K*-edges of absorption of lithium and oxygen, respectively. The PL emission spectra were measured by a 0.4 m vacuum monochromator (Seya–Namioka scheme) equipped with an microchannel plate-photomultiplier (MCP 1645, Hamamatsu). The PLE spectra were corrected using a photodiode AXUV-100 (International Radiation Detector Inc). The time-resolved measurements were performed in the same manner as described earlier, except for the time-window parameters. Two independent time-windows set for detection of luminescence signal within 0.8–6.3 ns (TW1) and 38.4–178.7 ns (TW2) were used. The PL emission spectra were not corrected to the transmission of the luminescence detection system.

The PL characteristics upon excitation in the UV spectral region from 3.0 to 6.0 eV were measured at 90 and 293 K at the laboratory of Solid State Physics of Ural Federal University. The 400 W deuterium discharge lamp with a continuous UV emission spectrum and the primary DMR-4 monochromator were used as an excitation source. The secondary DMR-4 monochromator and the R6328-10 (Hamamatsu) photomultiplier were used as registration system in the energy range of 1.5–5.0 eV. The PLE spectra were normalized to an equal number of photons incident on the sample using yellow lumogen with the energy-independent quantum yield over the studied spectral range. The PL emission spectra are shown without correction. Differences in the transmission spectra of registration systems for synchrotron spectroscopy, and for laboratory measurements, caused a small systematic shift between the maxima of PL emission bands recorded at different experimental setups. This shift is taken into account when discussing the results.

3. Experimental results

The goal of this section is to provide the most comprehensive set of spectroscopic data on LGBO:Ce for further discussion in the next section. The section presents the results of luminescence spectroscopy upon selective photoexcitation in the energy range from 3 to 650 eV. The lowest energy for intracenter excitation of Ce^{3+} ion determines the lower limit of the energy range, and the upper limit was chosen above the *K*-absorption edge of an oxygen atom, which is a host element of LGBO crystal. To cover the broad range of excitation energies we used different experimental setups. Spectroscopic results are presented in ascending order of excitation energy in this range. Identification of optical transitions in Ce^{3+} and Gd^{3+} ions has been carried out on the basis of the extended Dieke's diagram [13].

3.1. UV spectroscopy with a discharge lamp excitation

The excitation energy down to 3 eV is required to excite the lowest energy 4f–5d transitions in Ce^{3+} ion, however the SR excitation system does not cover the low-energy range. Because

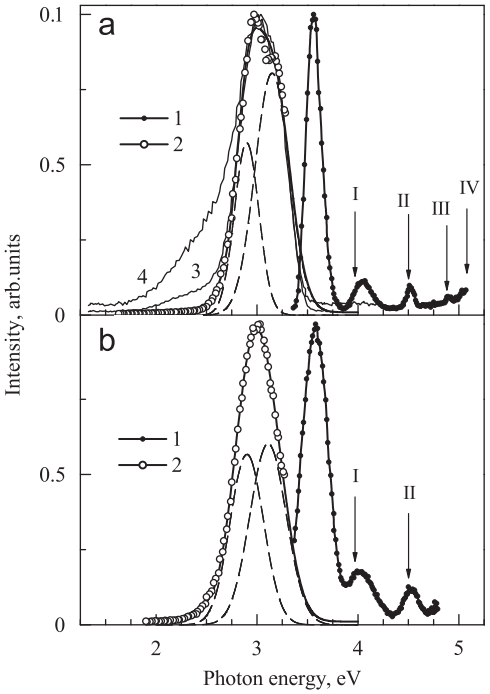

Fig. 1. The normalized PL and PLE spectra of LGBO:Ce crystals at 90—(a) and 293 K—(b). The PLE spectra were recorded monitoring emission at 3.0 eV—(1) and the PL emission spectra were recorded upon excitation at 3.55—(2), 4.0—(3) and 4.5 eV—(4). The elementary Gaussian bands are shown by dashed lines. Roman numerals indicate the optical transitions in Gd^{3+} ion from the ground level $^8S_{7/2}$ to the excited states of ^6P_j–(I), ^6I_j–(II), $^6D_{9/2}$–(III), and $^6D_{1/2,\ 7/2,\ 3/2,\ 5/2}$–(IV).

Table 1
Parameters of the PL emission spectra in the energy range of 2.0–3.5 eV: the energy positions of the doublet band maxima (E_{m1}, E_{m2}), the FWHMs of these bands, the intensity of the dominant band in the doublet normalized to 100 arbitrary units at the observed PL emission maximum (A), temperature (T), and distance between the doublet band maxima $\Delta E = E_{m2} - E_{m1}$.

Parameter	Excitation energy (eV)					
	3.55	3.55	5.65	7.00	7.00	7.75
T (K)	90	293	9	9	293	9
E_{m1} (eV)	2.90[a]	2.90[a]	2.61	2.96	2.97	2.96
$FWHM_1$ (eV)	0.28	0.38	0.24	0.27	0.29	0.27
E_{m2} (eV)	3.15[a]	3.11[a]	2.87	3.21	3.20	3.20
$FWHM_2$ (eV)	0.40	0.42	0.36	0.16	0.25	0.23
A (arbitrary units)	100	100	100	1.5	30	7
ΔE (eV)	0.25	0.21	0.26	0.25	0.23	0.24

[a] Laboratory UV-source was used for this measurement. The energy position of the PL emission band maximum in this case is subject to a systematic shift with respect to synchrotron spectroscopy data because of differences in the transmission spectra of registration systems at different experimental setups.

of this, in the energy range of 3.0–5.0 eV a discharge lamp was used as a UV light source for selective excitation of the lowest energy optical transitions that lead to luminescence of Ce^{3+} and Gd^{3+} ions in LGBO:Ce crystals. The normalized PL and PLE spectra recorded at 90 and 293 K for various excitation energies E_{ex} are presented in Fig. 1. A broad (FWHM = 0.55 eV) complex band with maximum at 3.0 eV dominates in the PL emission spectrum at 90 K. More than 98.2% of the PL emission spectrum is caused by the partially overlapped doublet PL emission bands, which are observed in the energy range of 2.5–3.5 eV, Table 1. PLE spectrum of this doublet is composed of a dominant peak at 3.56 eV (FWHM = 0.19 eV) and two low-intensity peaks at 4.05 eV (FWHM = 0.19 eV) and 4.52 eV (FWHM = 0.10 eV) with peaks amplitudes of 10 and 7% of the dominant peak intensity. In addition there are two very low intensity peaks at 4.9 and 5.05 eV, Fig. 1. The minimum Stokes shift for the PL bands of this doublet is 0.4 eV, the point of intersection of the normalized PL and PLE spectra is located at 3.4 eV, Fig. 1.

The doublet PL bands completely determine the luminescence spectrum of LGBO:Ce in the energy range of 2.6–3.6 eV. Besides, a weak luminescence occurs in the low-energy region of the spectrum at 1.3–2.6 eV. At E_{ex} = 3.56 eV its contribution to the PL emission spectrum is less than 2%. The relative contribution of the additional emission increases with increasing the excitation energy E_{ex}, which indicate dissimilarity in PLE-spectra of the doublet and the low-energy PL emission. The low-energy PL has been investigated earlier in Ref. [4]. In this research work we will focus on studying the properties of the dominant PL doublet.

Upon heating LGBO:Ce crystal from 90 to 293 K the PL intensity at 3.0 eV decreased by 55%. At room temperature, the elementary doublet bands are broadened, and the distance ΔE between their maxima decreases from 0.25 eV at 90 K to 0.21 eV at 293 K, Table 1. In this case the observed PL emission band at 3.0 eV is narrowed to FWHM = 0.51 eV, and the PLE peak at 3.56 eV is broadened to FWHM = 0.31 eV, Fig. 1.

3.2. UV/VUV synchrotron spectroscopy

In the UV/VUV spectral range of 3.7–24 eV the PL excitation of LGBO:Ce at 8 and 293 K was performed at SUPERLUMI using synchrotron radiation.

3.2.1. PL emission spectra

Fig. 2 shows the PL emission spectra in the energy range of 2.0–5.0 eV recorded with a CCD-camera upon excitation of LGBO:Ce crystal at E_{ex} = 6.9 eV. All the PL emission spectra are normalized to unit of intensity at the maximum.

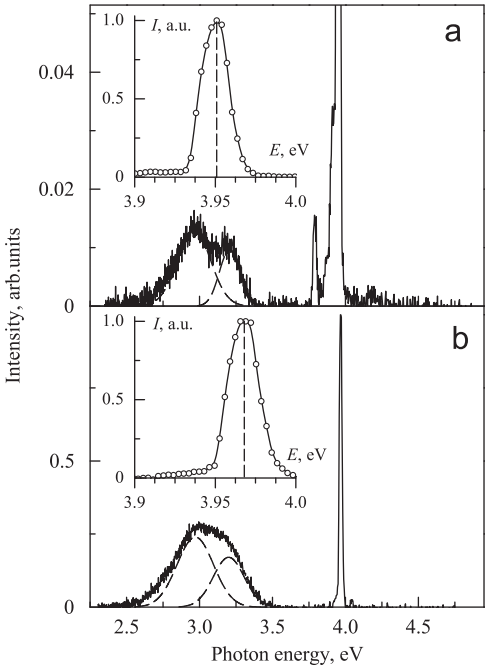

Fig. 2. The normalized PL emission spectra recorded for LGBO:Ce crystal at 9—(a) and 293 K—(b) upon excitation at 6.9 eV. The elementary Gaussian bands are shown by dashed lines. Insets show a larger scale fragments of the spectra in at 3.9–4.0 eV. The spectra are normalized to unit intensity at the maximum at 3.95–3.97 eV.

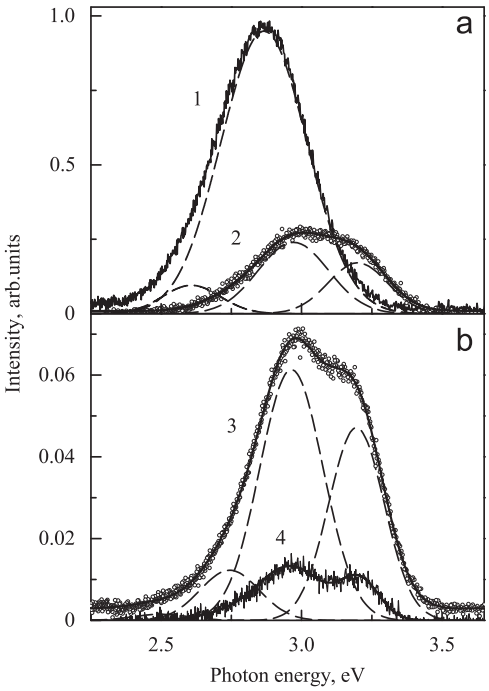

Fig. 3. The normalized PL emission spectra recorded for LGBO:Ce crystal at 9—(1,3,4) and 293 K—(2) monitoring emission at 5.65—(1), 6.98—(2), 7.75—(3) and 6.98 eV—(4). The elementary Gaussian bands are shown by dashed lines. The spectra are normalized to unit intensity at the maximum at 2–5 eV.

The narrow (FWHM = 0.020 eV) peak at 3.95 eV dominates in the PL emission spectrum of LGBO:Ce at 9 K, Fig. 2. This peak is due to the $^6P_j \rightarrow {}^8S_{7/2}$ transitions in the Gd^{3+} host ion. Another narrow (FWHM = 0.024) low-intensity peak of 3.79 eV is directly

adjacent to the main PL peak at 3.95 eV. The doublet PL emission bands are observed in the energy range of 2.5–3.5 eV. Spectroscopic parameters of the doublet bands are shown in Table 1. The intensity of the additional luminescence bands is less than 1.5% of the main peak intensity at 3.95 eV. Flat background is observed at energies above 4.0 eV, and its intensity does not exceed 0.1% of intensity for the main PL peak. It is important to emphasize that this weak emission can not be explained as the CCD background.

At 293 K the main peak of the Gd^{3+} PL is observed at 3.97 eV (FWHM=0.023 eV). Upon heating the relative intensity of the PL doublet bands, Table 1 increases up to 20 times and amounts to 30% of the amplitude of the main PL peak, Fig. 2.

Fragments of the PL emission spectra for the region of 2.25–3.60 eV, recorded for various excitation energies are shown in Fig. 3. The parameters of the elementary Gaussian-shaped bands are shown in Table 1. Most of the PL light sum in this spectral region is concentrated in the doublet of the Gaussian-shape elementary sub-bands with the inter peaks distances ΔE ranging from 0.21 to 0.23 eV at 293 K and from 0.24 to 0.26 eV at 9 K, Table 1.

The PL emission spectrum recorded at $E_{ex}=5.64$ eV and $T=9$ K, differs substantially from the previously discussed low-temperature PL spectra. The Gd^{3+} PL emission band in this spectrum is not detected, but there is only one broad complex PL band at 2.86 eV (FWHM=0.38 eV), Fig. 3. Decomposition revealed two elementary Gaussian-shaped sub-bands, Table 1, which accounted for 92.3 ($E_m=2.87$ eV) and 6.2% ($E_m=2.62$ eV) of the light sum, respectively. The total contribution of all the other luminescence bands is less than 1.5%.

At higher excitation energies in the PL spectrum of LGBO:Ce, there is also the peak of Gd^{3+} luminescence at 3.95–3.97 eV, which complements the discussed doublet of the PL emission bands in Fig. 2. In this case the PL spectrum profile in the 2.25–3.60 eV region depends weakly on the excitation energy and temperature, but there is only a change in its intensity, Fig. 3. From Table 1 it follows however that a slight narrowing of the high-energy PL band in the doublet occurs at the lowest levels of PL intensity.

3.2.2. PL excitation spectra

The PLE spectra TW1, TW2 and TI for the crystal LGBO:Ce at 9 and 293 K were recorded in the excitation energy range of 3.7–24 eV monitoring emissions at 3.0 and 3.95–3.97 eV. All PLE spectra for intrinsic Gd^{3+} emission at 3.95–3.97 eV are normalized to unity in the observed excitation maximum at $E_{ex}=6.6$–6.9 eV. The normalized PLE spectra TW1, TW2 and TI for the emission band in each case completely coincide with each other in profile. In this regard, only the time-integrated (TI) PLE spectra for the PL band at 3.95–3.97 eV are presented in Figs. 4–6. Time-resolved PLE spectra TW1 and TW2 of the 3.0 eV emission band are normalized for better visibility to coincidence their intensities with the PLE spectra of the Gd^{3+} luminescence in the energy range of 9–21 eV.

The overview PLE spectra recorded for LGBO:Ce at 9 K monitoring emission at 3.0 and 3.95 eV are presented in Fig. 4. It is possible to allocate three characteristic, partially overlapped areas on the PLE spectra that roughly correspond to the excitation energy ranges of 3.7–6.4 eV, 6.4–9.0 eV and 9–24 eV. Let us consider each area in more detail.

Energy range of the f–f *transitions in* Gd^{3+}: Fragments of the PLE spectra for the first energy range of 3.7–6.4 eV are shown in Fig. 5. This energy region corresponds to the f–f transitions in Gd^{3+} host ion. Roman numerals in Fig. 5 denote optical transitions in Gd^{3+} ion.

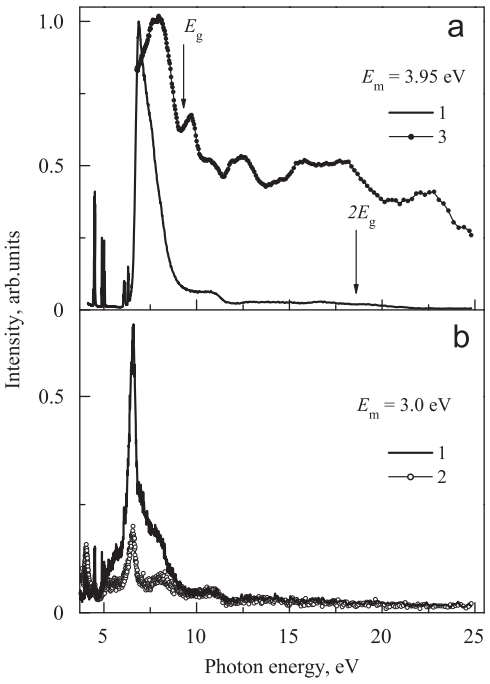

Fig. 4. The normalized PLE spectra recorded for LGBO:Ce crystal at 9 K monitoring emission at E_m in time-windows TW1—(2) and TW2—(1). The reflection spectrum at 9 K—(3). The notation E_g corresponds to the estimate value of the bandgap of LGBO crystal at 9 K.

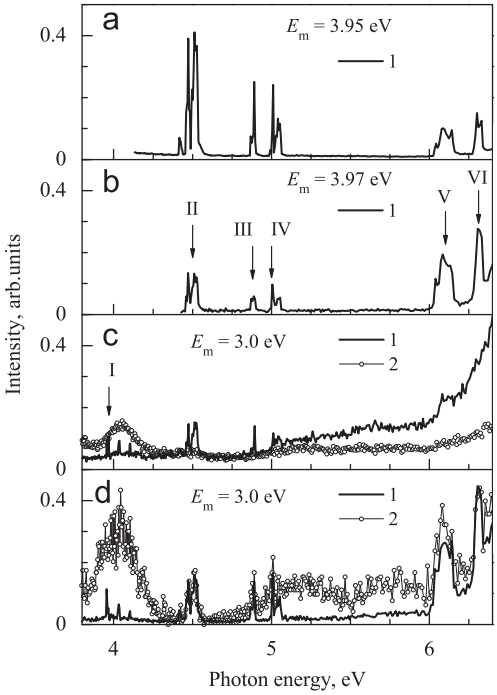

Fig. 5. Fragments of the normalized PLE spectra recorded for LGBO:Ce crystal at 9—(a,c) and 293 K—(b,d) monitoring emission at E_m in time-windows TW1—(2) and TW2—(1). Roman numerals indicate the optical transitions in Gd^{3+} ion from the ground level $^8S_{7/2}$ to the excited states of ^6P_j–(I), ^6I_j–(II), $^6D_{9/2}$–(III), $^6D_{1/2,\ 7/2,\ 3/2,\ 5/2}$–(IV), $^6G_{7/2}$–(V), and $^6G_{3/2,\ 13/2}$–(VI).

PLE spectrum of the 3.95 eV emission band at 9 K contains only a group of lines due to transitions from the ground $^8S_{7/2}$ level to excited states of ^6I_j–(II), $^6D_{9/2}$–(III), $^6D_{1/2,\ 7/2,\ 3/2,\ 5/2}$–(IV), $^6G_{7/2}$–(V) and $^6G_{3/2,\ 13/2}$–(VI). Only in the vicinity of the V and VI PLE bands there is a small contribution from the continuous spectrum. When heated at 293 K the qualitative picture is preserved,

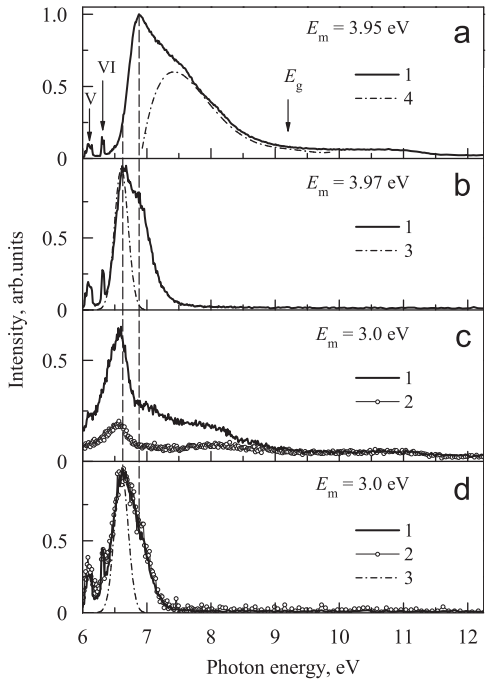

Fig. 6. Fragments of the normalized PLE spectra recorded for LGBO:Ce crystal at 9—(a,c) and 293 K—(b,d) monitoring emission at E_m in time-windows TW1—(2) and TW2—(1). The differential spectra were obtained as the absolute value of a difference for the curves (a) and (b) in the energy range from 6 to 7 eV—(3) and from 7 to 10 eV—(4). Roman numerals indicate the optical transitions in Gd^{3+} ion from the ground level $^8S_{7/2}$ to the excited states of $^6G_{7/2}$—(V) and $^6G_{3/2,\ 13/2}$—(VI). The notation E_g corresponds to the estimate value of the bandgap of LGBO crystal at 9 K.

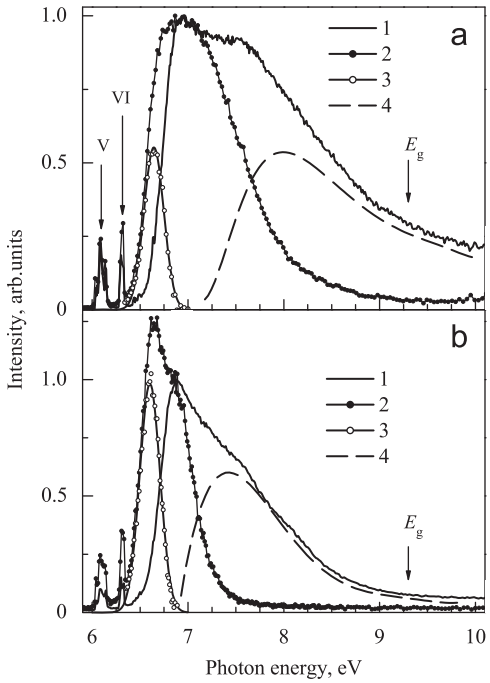

Fig. 7. Fragments of the normalized PLE spectra recorded for LGBO:Ce (0.5%)—(a) and LGBO:Ce (4.5%)—(b) crystals at 9—(1) and 293 K—(2) monitoring emission at 3.95—(1) and 3.97 eV—(2). The differential spectra were obtained as the absolute value of a difference for the curves (1) and (2) in the energy range from 6 to 7 eV—(3) and from 7 to 10 eV—(4). Roman numerals indicate the optical transitions in Gd^{3+} ion from the ground level $^8S_{7/2}$ to the excited states of $^6G_{7/2}$—(V) and $^6G_{3/2,\ 13/2}$ —(VI). The notation E_g corresponds to the estimate value of the bandgap of LGBO crystal at 9 K.

but there is a redistribution of intensity between the two groups of lines: bands II–IV are reduced in intensity by several times, whereas the intensities of the V and VI bands accordingly increased. In the energy region above 6 eV the continuous spectrum contribution increases monotonically with increasing excitation energy, Fig. 5.

PLE spectrum TW2 recorded at 9 K monitoring emission at 3.0 eV is a weakly structured: it contains several groups of low-intensity lines in the area of the I–IV bands and insignificant 'hump' in the area of the V band. A continuous PLE spectrum has a low intensity at 3.7–5.0 eV, increases monotonically at 5.0–6.0 eV, and increased sharply at energies above 6.0 eV, Fig. 5. PLE spectrum TW2 recorded at 293 K monitoring emission at 3.0 eV comprises several groups of intense lines located in the vicinity of I–VI bands. In the energy range of 4.2–6.4 eV the PLE spectrum coincides in profile with the PLE spectrum recorded at 293 K monitoring intrinsic PL emission at 3.97 eV, Fig. 5.

PLE spectrum TW1 recorded monitoring emission at 3.0 eV is markedly different from the previous case. At 9 K the spectrum does not contain specific groups of narrow lines, but instead there are a relatively broad PLE-band at 4.1 eV (FWHM = 0.20 eV) and continuous spectrum, which coincides with a continuous spectrum TW2 at 4.2–5.0 eV, and follows its profile with less intensity at 5.0–6.4 eV. At 293 K the spectrum consists of intense broadband at 4.1 eV (FWHM = 0.26 eV) and broad partially overlapping bands at 4.5–6.0 eV. Superimposed on this continuous spectrum is groups of narrow lines being similar to lines in the spectrum TW2. At energies above 6.0 eV the TW1 and TW2 spectra coincide in profile with each other, Fig. 5.

Energy range of charge transfer transitions. Fragments of PLE spectra for the energy range of 6.0–12.2 eV are shown in Fig. 6. The PLE spectrum recorded at 9 K monitoring emission at 3.95 eV comprises a dominant broad asymmetric band in the energy range from 6.0 to 8.5 eV with a maximum at 6.88 eV. The emission intensity increases dramatically at the low-energy slope of this PLE-band (6.5–6.8 eV) and gradually decreases at its high-energy slope (6.9–8.5 eV). At 293 K a high-energy slope of this band terminates already at 7.2 eV, and superimposed on the low-energy slope there is a new intense narrow band with a maximum at 6.6 eV, Fig. 6.

The narrow band at 6.6 eV (FWHM = 0.49 eV) dominates in the PLE spectra recorded monitoring emission at 3.0 eV. At 293 K, only this band appears in the PLE spectra TW1 and TW2 over the energy range of 6.4–12.2 eV. At 9 K, the 6.6 eV band also dominates. In the PLE spectrum TW1, this band is unique, but in the spectrum TW2, superimposed on this band the less intense broadband at 6.5–8.5 eV is observed being comparable in the energy position with the 6.88 eV band in the PLE spectrum of intrinsic luminescence.

Fragments of the normalized PLE spectra recorded for the crystals LGBO:Ce (0.5%) and LGBO:Ce (4.5%) at 9 and 293 K monitoring emission at 3.95–3.97 eV are shown in Fig. 7. The spectra are normalized to unit of intensity at 6.88 eV. Differential spectra obtained by subtracting the PLE spectra recorded at 9 and 293 K, are presented for each crystal. From the differential spectra, Fig. 7 it follows that the heating from 9 to 293 K leads to the appearance of the 6.6 eV band (FWHM = 0.25 eV) in the PLE spectra. Simultaneously, the broad asymmetric low-temperature band at 7–10 eV undergoes to the thermal quenching. Comparison of the differential spectra, obtained for crystals with different concentrations of the cerium impurity indicates that with increasing the impurity concentration increases the amplitude of the high-temperature band at 6.6 eV, whereas its energy position and FWHM remained unchanged. With an increase in the cerium impurity concentration from 0.5 to 4.5% of the maximum position of the low-temperature band shifts from 8.0 to 7.4 eV, and the FWHM decreases from 1.8 to 1.1 eV, Fig. 7.

Energy range of interband transitions: PL intensity is low when excited in the energy range of 9–24 eV. The most pronounced

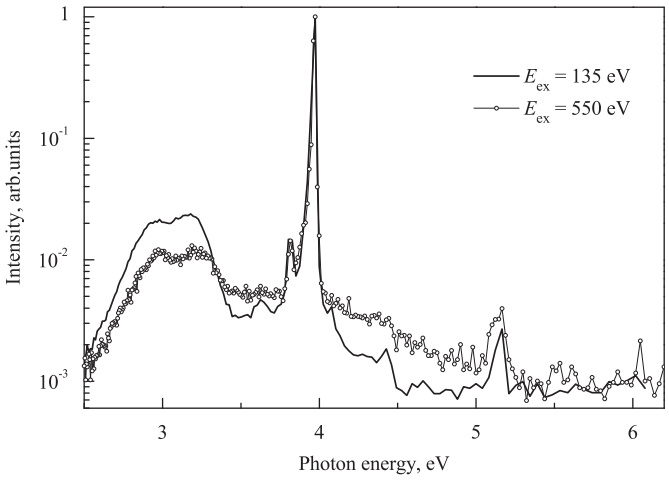

Fig. 8. The PL emission spectra recorded for LGBO:Ce crystal at 6 K upon excitation at 135 and 550 eV.

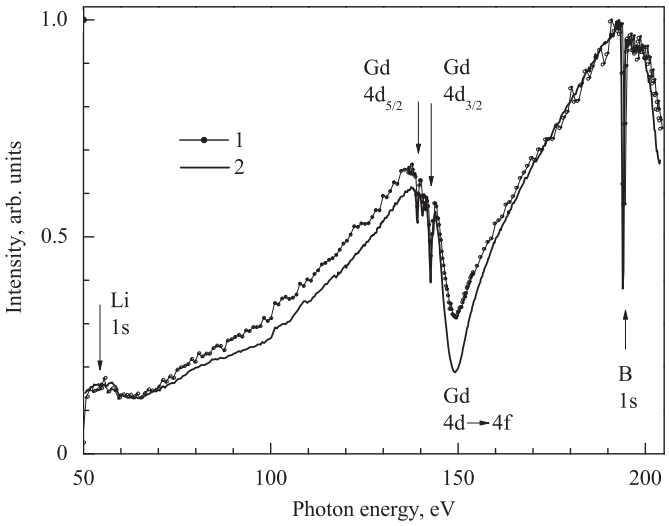

Fig. 9. The normalized PLE spectra at 50–210 eV recorded for LGBO:Ce crystal at 6 K monitoring emission at 3.0—(1) and 3.95 eV—(2).

structure is shown in the PLE spectra recorded at 9 K monitoring emission at 3.95 eV: at 9–11 eV the intensity remains constant at about 6% of the maximum at 6.88 eV; at 11–11.5 eV the intensity gradually decreases to 2% and then remains at this level up to 20 eV; at 20–22 eV the intensity decreases to undetectable level, Fig. 4. PLE spectrum recorded at 9 K monitoring emission at 3.0 eV also matches this description, only transitions between the levels of intensity are less pronounced. At 293 K, the PLE spectra of both bands have negligible intensity over all the energy range from 7.5 to 24 eV, Figs. 4 and 6.

3.3. XUV synchrotron spectroscopy

Figs. 8–10 show the results of the study of ultraviolet luminescence of LGBO:Ce crystals recorded monitoring in the range of 2.5–6.8 eV upon selective excitation by XUV-photons in the region of ultrasoft X-ray 50–220 eV and 500–650 eV, corresponding to the *K*-edges of absorption for lithium, boron and oxygen. Measurements were carried out at two fixed temperatures of 6 and 293 K. By studying the spectra, we have recorded in each case the time-resolved spectra in the time windows TW1, and TW2, and the time-integrated spectrum TI. We found that spectra

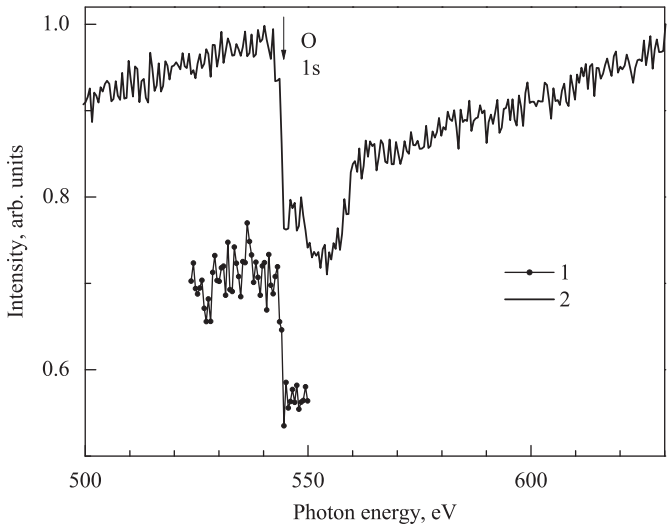

Fig. 10. The normalized PLE spectra at 500–630 eV recorded for LGBO:Ce crystal at 6 K monitoring emission at 3.0—(1) and 3.95 eV—(2). Curve (1) for better visibility was shifted down to 0.23 on the ordinate.

TW1, TW2 and TI in all cases coincide with each other in profile, in this regard, only the TI spectra are shown in Figs. 8–10.

From Fig. 8 it is seen that the emission spectrum at XUV excitation consists of narrow intensive line at 3.95 eV, which belongs to the radiative transitions in the Gd^{3+} ($^6P_j \rightarrow {}^8S_{7/2}$), and wide band at 3.0–3.2 eV, which has approximately 100 times smaller intensity and is due to 5d→4f transitions in Ce^{3+}.

The PLE spectra recorded for the crystal LGBO:Ce at 6 K monitoring emission at 3.0 and 3.95 eV are shown in Figs. 9 and 10. The PLE spectra of these two bands are similar. By varying the energy of exciting photons from E_{ex}=50 eV, a small decrease in intensity is observed at 57–59 eV. This shallow dip is comparable to the 1 s fundamental absorption edge of Li atoms. It is not intensive, and no fine structure was resolved in this experiment.

When the energy increases further, the PL intensity increases monotonically and reaches a smooth maximum at 137 eV. Two narrow dips at 139.2 and 142.8 eV are associated with the $4d_{5/2}$ and $4d_{3/2}$ absorption lines of gadolinium. A significant decrease in intensity occurs in 145–160 eV with a minimum at 148–150 eV. It is comparable to the 4d→4f transitions of gadolinium.

In the region 165–194 eV there is a smooth increase in the PL intensity, ending with an intense narrow dip at 194.5 eV. This dip is comparable to 1 s edge of boron and associated with electronic transitions from a core 1 s level of the boron atom to the conduction band (CB) of a crystal. Such transitions were observed earlier in the PLE spectra of intrinsic luminescence in lithium borate crystals LiB_3O_5 [14,15] and $Li_2B_4O_7$ [16]. The main difference in the profiles of the observed spectra in Fig. 9 is the ratio of luminescence intensities at the boundaries of a broad dip at 137–149 eV and 160–170 eV. Upon excitation at specified intervals the Ce^{3+} emission intensity is much higher than that for Gd^{3+} ion, Fig. 9.

The PLE spectra recorded upon excitation over the energy range of the 1 s fundamental absorption edge of oxygen atoms monitoring emissions at 3.0 and 3.95 eV demonstrate a sharp decrease by 25% of intensity at 544 eV, Fig. 10.

3.4. PL decay kinetics

The normalized PL decay kinetics curves recorded for LGBO:Ce crystal at T=9 and 293 K upon selective excitation at various energies ranging from E_{ex}=4 to 550 eV monitoring emission at 3.0 eV are shown in Fig. 11. Lifetime is short, but decay kinetics

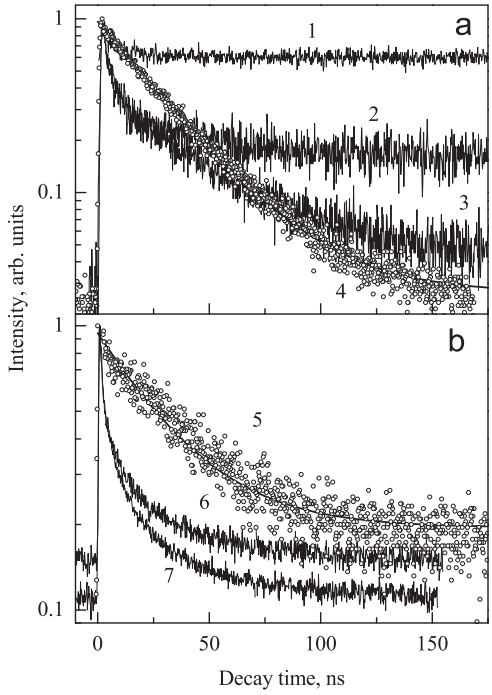

Fig. 11. The PL decay kinetics recorded for LGBO:Ce crystal at 9—(1–3, 6, 7) and 293 K—(4, 5) monitoring emission at 3.0 eV upon excitation by UV photons—(a) at 6.2–8.6—(1), 5.23—(2), 4.0–4.2—(3, 4) and VUV/XUV-photons—(b) at 15—(5), 550—(6) and 135 eV—(7).

curves could not be approximated by a single exponential law and have slow components. The formal decomposition of these curves revealed two fast exponential components with time constants of 3 and 27 ns, and a constant level—a pedestal summarizing the contribution of the inertial decay components of the micro- and millisecond time-range. The lifetime of $\tau = 27$ ns was observed only at 293 K, in the other cases the lifetime was ca. 3 ns. The contribution of the pedestal is maximal at the excitation energy of 6.2–8.6 eV.

4. Discussion

The purpose of this section is to determine the electronic structure parameters, such as the bandgap, minimal energy of the d–f and charge transfer transitions, the ground state locations of the 4f and 5d energy levels of divalent and trivalent lanthanide ions in the LGBO host lattice, using all available spectroscopic data on LGBO:Ce obtained in previous section as well as the known literature data.

4.1. *Electronic structure of LGBO and* $4f^n \rightarrow 4f^{n-1}5d-$transitions

In this paper, the bandgap of LGBO crystal has been determined from the spectrum of low-temperature reflection recorded at 9 K for the polished surface of the crystal LGBO:Ce, Fig. 4. The spectrum has a maximum at 8 eV and a sharp decline, ending in a local minimum at 9 eV. Comparison of the reflection spectrum with those of other borates, such as LiB_3O_5 and $Li_2B_4O_7$ [17], gives an approximate estimate of the low-temperature band gap of LGBO:Ce as $E_g = 9.3$ eV.

The intrinsic lowest energy electronic excitations in luminescent materials are usually due to electronic transitions from the valence band (VB) states onto the CB bottom. The probability of such transitions is determined by the nature of the initial and final electronic states. According to various sources, the low-energy tail

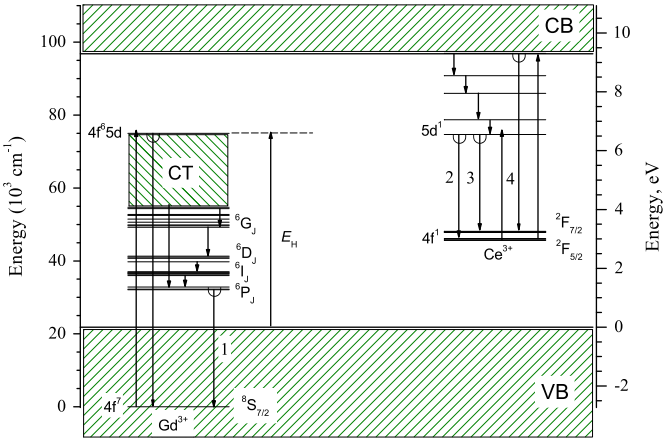

Fig. 12. Diagram of the relaxation of low-energy electronic excitations in the crystal LGBO: Ce. The numbers indicate the radiative transitions of $^6P_j \rightarrow {}^8S_{7/2}-(1)$, $4f^6 5d^1 \rightarrow {}^8S_{7/2}-(4)$ for Gd^{3+} ions, and $5d^1 \rightarrow {}^2F_{5/2}-(2)$, $5d^1 \rightarrow {}^2F_{7/2}-(3)$ for Ce^{3+} ion.

of the fundamental host absorption of borates crystals of the alkali and alkaline-earth metals occurs at 6.7 (β-BaB_2O_4 [18]), 7.75 ($(Gd,Y)BO_3$ [19]), 8.0 (LiB_3O_5 and $Li_2B_4O_7$ [17]), and 8.4 eV ($SrZr(BO_3)_2$:Eu [20]). As for LGBO crystals, we are not aware of publications on the VUV-absorption in the expected energy region of the host absorption edge of this crystal. The PLE spectra of intrinsic emission in LGBO crystal, Fig. 4 also can not help to reveal the host absorption edge, as it can be done in many other crystals, for example, LiB_3O_5 and $Li_2B_4O_7$ [17]. In this connection, the position of the low-energy tail of the fundamental absorption E_a was estimated by the empirical formula [21]

$$E_g \approx 1.08 \times (E_a + 0.2 \text{ eV}). \quad (1)$$

Assuming that $E_g = 9.3$ eV, from (1) it should be $E_a \approx 8.4$ eV, which agrees well with the above data for other borates. In many orthoborate crystals, the dominant contribution to the VB top is due to hybridized O 2p-, and B 2p-orbitals with prevailing the oxygen states [22]. Electronic structure of LGBO crystal in the vicinity of the VB top is also due to hybridized O 2p-, and B 2p-orbitals dominated by the oxygen states [23].

We are not aware of research works on the electronic structure of the LGBO conduction band, so we have to discuss the comparative data for other borates. The CB bottom in many borate compounds consists of antibonding hybridized O 2p-, and B 2p-orbitals, and d-orbitals of the metal cations [22]. The result is a mixed *pd*-character of the lowest-energy electronic excitations, which is manifested in the absence of pronounced excitonic states in the energy range of the low-energy tail of the fundamental absorption of a crystal. For example, the CB bottom in Sc_2O_3 is formed by 3d-orbitals of scandium, and the VB top resulted from 2p-orbitals of oxygen, so in this crystal, in contrast to the isostructural compound Y_2O_3, no excitonic absorption or exciton luminescence is observed [24,25]. Barium metaborate β-BaB_2O_4 also exhibits no excitonic states in the energy range of the low-energy tail of the fundamental absorption [18,26]. Indirect indications of the significant contributions of d-states of the metal cations to electronic structure of the CB bottom can be no manifestation of excitonic states in both the reflection and PLE spectra of LGBO over the energy range of 8.4–9.3 eV, Figs. 4 and 6, as well as the calculations [27] and the experimental data [28] on the electronic structure of similar compound $Ca_4GdO(BO_3)_3$.

The energy transfer processes in many borates of alkali metals are mainly determined, by the excitation of anion excitons and their migration along the continuous boron–oxygen framework, which is the principal element of the crystallographic structure in

Table 2
Energy parameters (eV) for Ln^{3+} (Ln=Ce, Eu, Gd) ions, calculated in this work for LGBO crystal (unlabeled data), and the available experimental data on these ions (labeled data) relating to the minimum energy of the $4f^n \rightarrow 4f^{n-1}5d$ transitions (ΔE_{fd}), the charge-transfer energy for $O^{2-} \rightarrow Ln^{3+}$ transitions (E_{CT}), the energy position of the low-energy edge of H-band (E_H), the energy positions of the 4 f^n ground states relative to the valence band top of LGBO crystal (E_f).

Parameter	Rare-earth ions		
	Ce^{3+}	Eu^{3+}	Gd^{3+}
ΔE_{fd}[a]	6.12[a]	10.57[a]	11.80[a]
ΔE_{fd}	3.56[b]	8.00	9.25
E_{CT}	8.50	4.63[c]	8.95
E_H	–	–	6.55[b]
E_f	3.00	−1.47	−2.70

[a] The data for free Ln^{3+} ions were taken from Ref. [13] and are presented for comparison.
[b] The experimental data obtained in this work for LGBO:Ce.
[c] This value was taken from our previous work [1].

the compounds, such as LiB_3O_5 and $Li_2B_4O_7$ [17]. Features of the LGBO crystallographic structure cause specific electronic structure and transport mechanisms for the lowest-energy electronic excitations. Energy transfer in the LGBO crystal occurs through the migration of cation excitons along continuous chains of the Gd^{3+} host ions [2,3,23]. To further refine the LGBO electronic structure and to determine the ground state positions of the lanthanide ions in the LGBO we will use the experimental data on luminescence spectroscopy, obtained in this work. The final result of this refinement is shown in Fig. 12. Let us consider in more detail the key stages in the construction of this diagram.

Electronic structure of free lanthanide ions (Ln) is well known, studied in detail and its description can be found in various publications and monographs, see e.g. [29]. Inner 4f-shells of the lanthanides are well shielded from external influences. Electronic energy structure of 4f-states is described by the extended Dieke's diagram [13]. When placing the Ln-ion into a host lattice, the positions of the 4f-levels vary only in the range up to 100 cm^{-1} (ca. 0.01 eV). In this connection to characterize the 4f-states of the Ln ion in most cases it is sufficient to determine only the position of its $4f^n$ ground state in the crystal (where n is the number of electrons in 4f-shell). The 4f ground state of divalent Ln^{2+} ions can be located in the CB or the band gap above the Fermi level. The ground 4f-state of trivalent Ln^{3+} ions can be located in the band gap below the Fermi level or in VB. For example, in $SrAl_2O_4$:Gd^{3+} crystal the $4f^7$ ground state of Gd^{3+} ion is located at 3.0 eV below the VB top [30]. The position of the 5d excited level of trivalent lanthanide with respect to its 4f ground state in inorganic materials is strongly influenced by the crystalline environment and may vary from crystal to crystal in the tens of thousands of cm^{-1} (ca. several few electron volts). The minimum energy of the $4f^n \rightarrow 4f^{n-1}5d$-transition ($\Delta E_{fd}$) for the Ln^{3+} ion in the crystal can be determined by the formula [31]

$$\Delta E_{fd} = \Delta E^a_{fd} - D, \quad (2)$$

where ΔE^a_{fd} is a minimal energy for the $4f^n \rightarrow 4f^{n-1}5d$ transition in a free Ln^{3+} ion, Table 2; D is the spectroscopic red shift. According to our experimental data, the minimum energy of $4f^1 \rightarrow 5d$ transition for Ce^{3+} ion in the LGBO crystal is $\Delta E_{fd} = 3.56$ eV (28 713 cm^{-1}), Fig. 1. Substituting this value in (2), we define the red spectroscopic shift for LGBO crystal as $D = 20.6 \times 10^3$ cm^{-1}. The value of the red spectroscopic shift D is a characteristic parameter of the host crystal, D is determined only by the crystal properties and remains the same for any Ln^{3+} ions in this crystal. From the known value of D we have calculated by the formula (2) the minimal energies of $4f^n \rightarrow 4f^{n-1}5d$-transitions for Eu^{3+} and Gd^{3+} ions in the LGBO crystal, Table 2. The calculated energy values fall into the energy region of fundamental absorption of LGBO crystal and therefore could not be measured experimentally.

4.2. Charge transfer transitions

The electron transfer from the valence band states of a crystal onto the unfilled f or d-orbital of the metal cation leads to the charge transfer (CT) electronic transition. Such transitions are partially allowed and appear in the UV and VUV spectral region as a broadband of optical absorption. The CT band parameters depend on the electronegativity of the ligands, the electron affinity of the cations and the distance between the cation and the ligand. The minimum energy of CT-transition during optical absorption is determined by formula [32]

$$E_{CT} = (\chi(O) - \chi(Ln)) \times 3.72 \text{ eV}, \quad (3)$$

where χ(O) and χ(Ln) are the optical electronegativities of oxygen atom and Ln-cation. This relation is well satisfied for many rare-earth elements, such as Eu^{3+} ion. Two important facts have been empirically established for the crystalline hosts doped with europium ions. First, E_{CT} in these crystals corresponds to the energy position of the $4f^7$ ground level of the divalent Eu^{2+} ion relative to the VB top of the crystal; second, the $4f^7$ ground state of Eu^{2+} ion in these crystals is located at lower energy than the $4f^5 5d^1$ ground level of the trivalent Eu^{3+} ion [30,33]. In oxides, the CT transition $O^{2-} \rightarrow Eu^{3+}$ is due to electron transfer from the O 2p states of VB onto the $4f^7$ ground state of Eu^{2+} ion [21,34–36].

The broad optical absorption band at 4.5–7.0 eV in LGBO crystal is associated with CT-transition $O^{2-} \rightarrow Eu^{3+}$, and the low-energy edge of this band at 10 K is located at E_{CT}=4.63 eV [1,37]. In the framework of the model [21], for a E_{CT} known value for Eu^{3+} ion, we can calculate the E_{CT} values for all other Ln^{3+} ions in the same host lattice.

$$E_{CT} = E_{CT}(Eu) + \Delta E_{vf}(Ln), \quad (4)$$

where ΔE_{vf}(Ln) is a correction constant, which is mainly determined by the properties of the Ln^{3+} ion and only slightly depends on the crystal specificity. The values of the ΔE_{vf} constants for Ce^{3+} and Gd^{3+} ions are 3.87 and 4.32 eV, respectively [21]. The appropriate E_{CT} values for Ce^{3+} and Gd^{3+} ions in LGBO crystal were calculated and presented in Table 2.

The expected value of the minimum energy for CT-transition $O^{2-} \rightarrow Gd^{3+}$ in LGBO crystal is E_{CT}=8.95 eV, Table 2. Assessment by formula (3) with $\chi(O) = 3.2$ and $\chi(Gd) = 0.91$ [32] yields for Gd^{3+} ion a bit lower value of E_{CT}=8.52 eV. In any case, the energy of 8.95–8.52 eV corresponds to the low-energy tail of the fundamental absorption of LGBO, where the PLE spectra exhibit no peculiarities, which are usually typical for the excitation at the CT absorption band, Figs. 4–6. At the same time, a low-temperature broad PLE band with a maximum at 7.5–8.0 eV was presented in the differential spectra, Fig. 7. For comparison we present the experimental data for the (Gd,Y)BO_3 crystal, where the CT absorption band $O^{2-} \rightarrow Gd^{3+}$ was identified the PLE spectra at 7.47 eV [19].

The dominant band at 6.88 eV in the PLE spectra of LGBO, Fig. 6 exhibits all the properties, which are usually specific to excitation at the CT absorption band. However, in the light of the above analysis, its interpretation does not seem a simple and straightforward. In our opinion, the 6.88 eV band in LGBO crystal is due to an energy transfer from the boron–oxygen ligands to Gd^{3+} ion with participation of intrinsic lattice defects in the form of the hole radical BO_3^{2-}. The basic properties of complex oxyanions BO_3^{2-} have been previously studied in detail by many researchers using the methods of electronic paramagnetic resonance and optical absorption spectroscopy, see e.g. [38]. The BO_3^{2-} oxyanion in borate crystals is in some senses similar

Table 3
The energy positions (E_m) of the absorption bands detected in PLE spectra in the energy range of the expected charge-transfer transitions.

Crystal	E_m (eV)	Transition[a]	Reference
$BaZr(BO_3)_2$	6.20	BO_3^{2-}	[53]
$LaCa_4O(BO_3)_3$	6.63	BO_3^{2-}	[54]
$YCa_4O(BO_3)_3$	6.59	BO_3^{2-}	[54]
$SrAl_2B_2O_7$	6.78	BO_3^{2-}	[53]
$SrZr(BO_3)_2$	7.13	BO_3^{2-}	[20]
$YAl_3(BO_3)_5$	7.25	BO_3^{2-}	[53]
$Ba_3Gd(BO_3)_3$:Ce	6.36	BO_3^{2-}	[39]
$GdCa_4O(BO_3)_3$	6.74	BO_3^{2-}	[54]
$Y_{0.65}Gd_{0.35}BO_3$	7.05	BO_3^{2-}	[53]
$La_2O_2CO_3$	6.36	CO_3^{2-}	[55]
$Gd_2O_2CO_3$	6.70	CO_3^{2-}	[55]
Gd_2SiO_5	6.97	O–Gd	[19]
$GdAlO_3$	7.29	O–Gd	[19]
$Gd_2O_2CO_3$	7.29	O–Gd	[55]
$GdBO_3$	7.47	O–Gd	[56]
$(Gd,La)Al_3(BO_3)_4$	7.90	O–Gd	[57]

[a] Interpretation of each transition follows corresponding reference.

to self-trapped hole. However, its formation requires the prior existence of a small lattice distortion that can occur near the rare-earth ions.

Optical absorption and PLE spectra of many complex borate crystals exhibit the so-called H-band, which is located in the energy range slightly lower than the low-energy tail of the host absorption and exhibit all the properties typical for CT-band. The H-band concept was first introduced by Dorenbos et al. [39] for the host PLE band in $Ba_3Gd(BO_3)_3:Ce^{3+}$, they pointed to the possible connection of this band with a complex oxyanion, but the true origin for this band in $Ba_3Gd(BO_3)_3$ has not been fully resolved. Table 3 contains the available data on the H and CT bands observed in PLE spectra of certain complex compounds. Let us discuss the properties of the H-band in more detail.

First, from Table 3 it follows that the energy position of the 6.88 eV band in LGBO, Fig. 6 is well comparable to that for the H-band in the other crystals.

Second, the H-band is observed not only in crystals containing Gd^{3+} ions, but also in crystals without gadolinium ions. This is consistent with assumption that the H-band is due to optical transitions in the BO_3^{2-} hole center. Indeed, the VB top states can be represented as a continuous network of the anionic BO_3^{3-} groups. Photoinduced electron transfer from VB onto a local level in the band gap occurs during excitation by VUV photons with energies less than E_g. A hole in the VB remains localized in the potential field of the localized electron and this hole can be represented as the BO_3^{2-} radical. Note incidentally that a similar scenario is realized in the electronic transitions with charge transfer $O^{2-} \rightarrow Ln^{3+}$.

Third, the H-band intensity in the PLE spectra increases by several times when Gd^{3+} ions are present in the crystal. This indicates the presence of efficient channel for energy transfer from BO_3^{2-} radical to Gd^{3+} ion. Two conditions are necessary for a high probability of the energy transfer: overlapping of wave function of the radical and Gd^{3+} ion, and the coincidence of the transition energies. These conditions are well satisfied for a number of the yttrium and gadolinium orthoborate crystals, where the energy of the charge-transfer transitions $O^{2-} \rightarrow Gd^{3+}$ overlaps with the energy of optical transitions in the BO_3^{2-} radical, see e.g. $(Gd,Y)BO_3$ crystal [19]. The carbonate crystals exhibit, apparently, a similar scenario involving a complex oxyanion CO_3^{2-}, Table 3.

In our opinion, a broad band with a maximum at 7.5–8.0 eV in the differential PLE spectra, Fig. 7 can be interpreted as the CT absorption band $O^{2-} \rightarrow Gd^{3+}$, whereas the 6.88 eV dominant band in the PLE spectrum of LGBO:Ce should be interpreted as the H-band. In this work, we did not plan to develop a detailed mode to explain the high efficiency of the PL excitation in LGBO:Ce through the H-band. Let us only mention that the probable reason for this is that the $4f^6$5d-level of the trivalent Gd^{3+} ion in wide bandgap crystals are usually located in energy below the ground $4f^8$ level of the divalent Gd^{2+} ion, which is located in the same crystal either in the CB, or slightly below the CB bottom. For example, 4f-level of Gd^{2+} ion in the $SrAl_2O_4$ crystal is located at 2.4 eV above the $4f^6$5d-level of Gd^{3+} ion in the same crystal [30].

We can assume that in this case, the minimum energy of the CT transition $O^{2-} \rightarrow Gd^{3+}$ will correspond to the transfer of O 2p electron from the valence band states onto the $4f^6$5d-level of the trivalent Gd^{3+} ion. The results of quantum chemical calculations of electron transfer from the $KZnF_3$ ligand onto the 5d level of the Yb^{3+} ion testify in favor of such a possibility [40].

4.3. *Absolute location of* $4f^n$ *and* $4f^{n-1}5d$ *ground states in LGBO crystal*

From the PLE spectra of intrinsic luminescence at 3.95–3.97 eV, Fig. 7 it follows that the low-energy cut-off for the H-absorption band is located at $E_H = 6.55$ eV. In light of the discussion above, this value corresponds to the position of $4f^6$5d energy level of Gd^{3+} ion relative to the VB top in LGBO crystal. Therefore, the position of the $4f^7$ ground level of the Gd^{3+} ion relative to the VB top of LGBO crystal is $E_H - \Delta E_{fd} = 6.55 - 9.25 = -2.7$ eV, Table 2. This is consistent with the known data on the location of the $4f^7$ ground level of Gd^{3+} ion in various oxide, sulfide and fluoride materials [30,39,41]. Location of the $4f^8$ ground level of Gd^{2+} ion in LGBO crystal is $E_{CT} = 8.95$ eV (see Table 2), that exceeds the energy location of $4f^6$5d-level by the value of $E_{CT} - E_H = 2.4$ eV. This indirectly indicates the possible contribution of 5d-orbitals of the Gd^{2+} ion to the states of the CB bottom. In addition, the sharp drop in intensity is observed in the low-temperature reflection spectrum of LGBO at 8–9 eV, Fig. 4. A value of 8.95 eV is located in the energy interval corresponding to the low-energy tail of the fundamental absorption of LGBO crystal. The difference $E_g - 8.95 = 0.35$ eV is comparable in magnitude to the expected binding energy for the formation of excitons or electron–hole pairs upon excitation in the energy range of the low-energy tail of the fundamental absorption of a crystal. Such a correspondence was found previously for several other optical materials [21].

The $4f^1$ ground level of Ce^{3+} ion in wide bandgap crystals are usually located above the VB top. The model [21,30] describes the relationship between the energy values of the $4f^n$ ground states for different lanthanides situated in the same host lattice. If we know the energy of the $4f^n$ ground state for one rare-earth ion, the model can calculate the energies of the $4f^n$ ground state for other lanthanides in the same crystal. The $4f^7$ ground state of Gd^{3+} ion in LGBO crystal is located on 2.7 eV below the VB top, and the systematic shift between the $4f^n$ ground levels of Ce^{3+} and Gd^{3+} ions according to Ref. [21] is $\Delta E^{Gd,Ce} = 45\,800$ cm^{-1} (5.69 eV). In this case, the $4f^1$ ground state of Ce^{3+} ion in LGBO crystal should be located at $(5.69-2.7) \approx 3.0$ eV above the VB top, Table 2; Fig. 12. The $4f^1$ ground state of Ce^{3+} ion is split by spin–orbit interaction on the two levels of $^2F_{5/2}$ and $^2F_{7/2}$, Fig. 12. The splitting depends on many factors, and within a small range the splitting width varies depending on the temperature and excitation conditions. Table 1 shows that the values of splitting obtained in our measurements are quite close to the expected value of 0.25 eV [42].

In addition to the Ce^{3+} ions, the LGBO:Ce crystal also contains the Ce^{4+} ions associated with charge-compensating lattice defects. The possible charge-transfer transitions between the states of the VB top and a 4f vacant state of Ce^{4+} ion can also

be used to determine the location of the $4f^1$ ground state of Ce^{3+} ion in the crystal. However, from general considerations it is obvious that the energy of the $4f^1$ ground state of Ce^{3+} ion in the defect complex, will be somewhat higher than the energy of the same ion in a regular position in the defect-free region of the crystal. Indeed, the broad optical absorption band for the tetravalent Ce^{4+} ions in LGBO:Ce crystal starts at an energy of 3.2 eV and has a flat maximum at ca. 4 eV [43].

To determine the position of 5d-level of Ce^{3+} ion in LGBO crystal we use the experimental value of the minimum energy of the $4f^1 \rightarrow 5d$ transition for Ce^{3+} ion, which is equal to 3.56 eV, Fig. 1. Location of 5d-levels of Ce^{3+} ion in LGBO crystal should be at (3.0 + 3.56 eV)=6.56 eV above the VB top. The resulting value is close to the energy of 6.55 eV, established above for the $4f^6 5d$-level of Gd^{3+} ion in LGBO. This is not surprising because the location of the $4f^{n-1}5d$-level of lanthanides in the same host lattice is determined mainly by the crystal field and does not depend on the specificity of 4f-ion of the same charge state [21,30,33]. Once we have determined the energy positions of the ground levels of the Ce^{3+} and Gd^{3+} ions in LGBO, we can calculate using the model [21,31] the expected positions of the ground levels for all lanthanides in LGBO crystal. The results of calculation are shown in Fig. 13.

Absolute location of 4f ground states of the Gd^{3+} host ion can also be determined experimentally using photoelectron spectroscopy. We are not aware of the published photoelectron spectroscopy data for LGBO, however, such data are available for certain complicated oxides. Thiel et al. [44,45] have measured resonant photoemission of rare earth ions in aluminum garnets and found the absolute locations of 4f ground states of the ions relative to the VB top. Aluminum garnets and LGBO have different bandgaps, so the values of Ref. [44,45] can not be directly compared with our data on LGBO. The midway between the VB top and the CB bottom can be chosen as the reference level for such comparison because in perfect dielectric crystals the Fermi level is located here. For YAG crystals E_g=8 eV [46], and from the data of Ref. [45] we can obtain the positions of certain 4f elements below the bandgap midway level: 1.3–1.9 eV (Ce^{3+}) and 7.3–8.7 eV (Gd^{3+}). For LGBO crystal E_g=9.3 eV, and from Table 2 we can get the appropriate values of 1.65 eV (Ce^{3+}) and 7.35 eV (Gd^{3+}). It should be noted that the photoelectron spectroscopy data for YAG and the luminescence spectroscopy data for LGBO are quite consistent.

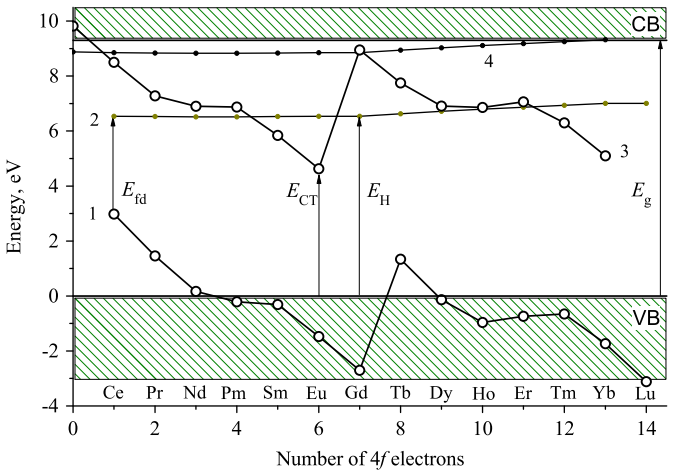

Fig. 13. The calculated energy level diagram of the lanthanides in LGBO depending on the number of electrons in the ground state of the $4f^n$-configuration of the trivalent lanthanide ion. Curves 1 and 2 correspond to the lowest states of the $4f^n$ and $4f^{n-1}5d$-configurations of the trivalent lanthanides. Curves 3 and 4 correspond to the lowest levels of the $4f^{n+1}$ and $4f^n5d$-configurations of the divalent lanthanides. The arrows show the experimental data used to construct the diagram.

4.4. Luminescence of LGBO:Ce upon UV/VUV excitation

Intrinsic luminescence of LGBO crystal at 3.95–3.97 eV is due to the $^6P_j \rightarrow {}^8S_{7/2}$ radiative transitions in the Gd^{3+} host ions. At 4.4 K the complex PL emission band consists of 10 lines of varying intensity, which is separated by a distance less than 0.1 nm [2]. It is obvious that the structure of these lines is beyond the spectral resolution of our optical equipment, but the observed shift of the energy position of the PL peak from 3.95 to 3.97 eV upon heating from 10 to 293 K in our measurements is due to different temperature dependence of these lines. We have detected no radiative transitions from the excited high-energy states of ^6I_j, ^6D_j and ^6G_j of Gd^{3+} ions in LGBO crystals. Two processes are responsible for the lack of the concentration quenching of the photoluminescence of the host Gd^{3+} ions in LGBO crystal. First, a fast diffusion of electronic excitation energy along the chains of Gd^{3+} ions occurs in LGBO crystal at temperatures above 40 K. The experimental data [2], and electronic structure calculations [23] showed essentially one-dimensional character of energy transport along the chains of Gd^{3+} ions. Second, a high probability of the transfer of electronic excitation energy to a neighboring Gd^{3+} ion in comparison with the process of radiative relaxation of energy on the initially excited Gd^{3+} ion [2,3]. Owing to the high degree of shielding of 4f-shell by the outer electronic shells, the PL decay kinetics in Gd^{3+} ion is rather slow, and at 293 K the lifetime can be up to 360 μs [2]. In our measurements such slow PL decay kinetics appears in the form of a pedestal.

In the energy region above 6.2 eV the luminescence excitation in LGBO crystal occurs through the CT transitions. In this case, the electron transfer from the VB top occurs either onto the $4f^6 5d$ level of Gd^{3+} ion (E_H), or the $4f^8$ level of Gd^{2+} ion (E_{CT}). The hole that remains in VB is localized in the neighborhood of the ion. De-excitation occurs through non-radiative recombination of an electron with the localized hole. The charge transfer luminescence in LGBO crystal is not realized because the charge-transfer state is located at the energy higher than that for the lowest excited $4f^{n-1}5d$ state of Gd^{3+} ion. Instead, the recombination energy is transferred to the Gd^{3+} ion, leading to its excitation. At a later stage there is either the excitation energy transfer along the chains of Gd^{3+} ions, or the rapid non-radiative relaxation to the lowest excited state of the ion, resulting in the $^6P_j \rightarrow {}^8S_{7/2}$ radiative transition in Gd^{3+} ion.

The $4f^6 5d \rightarrow 4f^7$ radiative transitions in the Gd^{3+} ion have not been experimentally observed, since the expected transition energy is 9.25 eV (see Table 2), which corresponds to the fundamental absorption region of the LGBO crystal.

Interconfigurational $5d^1 \rightarrow 4f^1$ radiative transition in Ce^{3+} ion is predominantly electric dipole transition and it appears as an intense doublet of broad overlapping emission bands with a short lifetime. The final stage of the radiative process is described by the scheme.

$$(Ce^{3+})^* \rightarrow Ce^{3+} + h\nu. \quad (5)$$

For the intracenter excitation of PL of Ce^{3+} ions, this scheme is the only possible one. In the low-symmetry crystal field, 5d states of Ce^{3+} ion are split, in addition to the lowest energy excited $5d^1$ state, there have also been highly excited states. In addition to the 3.56 eV band, corresponding to the $4f \rightarrow 5d^1$ optical transition, the PLE spectra of LGBO:Ce also show excitation bands at 4.1, 4.5, 5.2 and 5.6 eV, Figs. 1 and 5. Fast ($\tau < 1$ ns) non-radiative relaxation of an electron from any of a highly excited level to the lowest excited $5d^1$ state with the further realization of the (5) is characteristic of the electronic structure of Ce^{3+} ion. Therefore,

the emission spectrum of Ce^{3+} ion in LGBO crystal is determined only by the radiative transitions of $5d \rightarrow 4f^1$ from the lowest energy excited state [5].

The excitation of the impurity luminescence in LGBO crystal occurs through the transfer of electronic excitation energy along the chains of Gd^{3+} ions. This scheme results in efficient transfer of electronic excitation energy from the Gd^{3+} host ions to the Ce^{3+} impurity ions, since the PL emission spectrum of Gd^{3+} ion at 3.95–3.97 eV coincides well with the optical absorption band of the Ce^{3+} ion. In addition, the energy of the lowest excited state of Gd^{3+} ion (3.95–3.97 eV) is higher than that for the lowest excited 5d state of Ce^{3+} ion (3.56 eV), so the energy transfer in LGBO crystal occurs only in one direction $Gd^{3+} \rightarrow Ce^{3+}$ [2].

The impurity centers Ce1 and Ce2, which are the Ce^{3+} ion, replacing the Gd^{3+} host ion have previously been found in the crystal LGBO:Ce [4]. In the first case the Ce^{3+} ion is associated with a defect in the first coordination sphere, while in the latter case, the Ce^{3+} ion is located in the regular gadolinium site in a defect-free region of the crystal. These impurity related centers are slightly different in their spectral characteristics, so the observed spectrum of the impurity luminescence is due to the superposition of the PL emission spectra of the Ce1 and Ce2 centers [4]. The ratio of their contributions is determined by the degree of defectiveness of the crystal. Fig. 1 shows that the main contribution to the impurity luminescence is due to the Ce2 center, whereas the contribution of the Ce1 center, expected in the low-energy part of the spectrum is negligible. This demonstrates the high quality of the crystals studied.

The PL decay kinetics of LGBO:Ce upon selective excitation by UV and VUV photons is single exponential [1]. When excited by XUV photons the PL decay kinetics differs significantly from the single exponential decay law. A formal deconvolution revealed two components of the decay kinetics with lifetimes of 3 and 27 ns, which should be attributed to the $5d \rightarrow 4f$ transitions in Ce^{3+} ion. The component of the decay kinetics with the lifetime of ca. 27 ns is due to the $5d \rightarrow 4f$ radiative transitions in the Ce^{3+} ion, which is located in a defect-free area of a crystal, and corresponds to the Ce2 impurity center. The decay kinetics with the lifetime of ca. 3 ns refers to the same transitions in the Ce^{3+} ion associated with a defect, which corresponds to the Ce1 impurity center.

Only Ce2 centers can be excited during the energy transfer through the chains of Gd^{3+} ions, since at these centers the Ce^{3+} ion is situated in the regular gadolinium site in the defect-free region of the crystal. The PL emission spectrum under these conditions remains almost unchanged at varying the excitation energy and temperature, Fig. 3; Table 1. The direct photoexcitation leads to excitation of all Ce^{3+} ions contained in LGBO:Ce crystal. As a result, the PL emission spectrum is an intractable superposition of the emission spectra of different centers, which are composed of Ce^{3+} ions, Fig. 3.

In the direct photoexcitation of the Ce^{3+} impurity center in a crystal, the energy of exciting photons is limited to the interval from the minimum energy of $4f^1 \rightarrow 5d$ transition to a transition of an electron onto the autoionization states located just below the CB bottom. At the autoionization of an electron from the 5d excited state of the Ce^{3+} impurity ion onto the CB bottom, the electron remains localized in the potential field of the hole, located on the initial cerium ion. This is a geminate electron–hole pair, which is available for a direct radiative recombination by the scheme.

$$Ce^{4+} + e^- \rightarrow Ce^{3+} + h\nu. \quad (6)$$

The emission arising by the (6), is due to dipole-allowed transitions, and should have a fast decay kinetics. Its spectral composition should differ from the emission spectrum that arises during $5d^1 \rightarrow 4f$ transitions in Ce^{3+} ion. This emission sometimes referred to 'anomalous luminescence' and interpreted as excitation of impurity bound exciton [36,47], because it can be excited only in a very narrow range of energies of exciting photons: at lower energies, the transition of an electron from the impurity center state onto the CB bottom can not occur, and at higher energies, the electron at CB gets a large enough kinetic energy to overcome the potential barrier of the impurity center. Fast anomalous luminescence ($\tau < 10$ ns) with similar properties has been previously revealed experimentally in $Cs_3LuCl_6:Ce^{3+}$ crystals (PL emission band at 4.41 eV, FWHM = 0.46 eV, narrow PLE band at 5.8–6.2 eV) [48].

However, we observed no such emission in LGBO:Ce crystals upon excitation with UV and VUV photons. The probable reason for this is the 4.5 and 6.2 eV optical absorption bands due to optical transitions of $^8S_{7/2} \rightarrow {}^6I_j$ and $^8S_{7/2} \rightarrow {}^6G_j$ in the Gd^{3+} host ions, which coincide with the expected energy positions of the PL and PLE bands for proposed anomalous luminescence. At the same time, some indirect evidence indicates the existence of such a PLE mechanism in LGBO:Ce crystals. In our opinion, the dominant narrow band at 6.6 eV (FWHM = 0.49 eV) in the PLE spectrum at 3.0 eV is due to electron transfer from the $4f^1$ ground state of the Ce^{3+} ion onto the autoionization states near the CB bottom. High efficiency is due to the direct recombination according to (6) However, the anomalous luminescence is not observed, since there is an excitation energy transfer onto the ^6P_j and ^6I_j levels of Gd^{3+} ions. The usual scheme of excitation of Ce^{3+} ions through the energy transfer along the chains of Gd^{3+} ions is realized in the next stage. This is indicated by the presence of a pedestal in the decay kinetics of the Ce^{3+} luminescence upon excitation at 6.6 eV. Further confirmation of the possibility of such a scheme is the presence of high-temperature band at 6.6 eV (FWHM = 0.25 eV) in the differential PLE spectra of the Gd^{3+} emission, Fig. 7. The bandwidth is comparable to the magnitude of the spin–orbit splitting of the $4f^1$ ground states of Ce^{3+} ion, Table 1. At low temperatures, there is no energy migration along the chains of Gd^{3+} ions and the probability of energy transfer back to Ce^{3+} ion is sufficiently high. The migration of electronic excitations in the chain of Gd^{3+} ions occurs at temperatures above 40 K, it increases the probability of radiative relaxation on Gd^{3+} ions. The PL intensity at 3.0 eV upon excitation at 6.6 eV can be increased by heating because of the potential barrier for transition between the CB bottom and the excited 5d states of Ce^{3+} ion, as it take place in $Cs_3LuCl_6:Ce^{3+}$ crystals [48]. Note that the flat background at energies above 4 eV in Fig. 2 may be just a manifestation of the expected anomalous luminescence.

In the energy region above 6.6 eV, the luminescence of the Ce^{3+} impurity ion can be excited only by the energy transfer along the chains of Gd^{3+} ions. In the fundamental absorption region of a crystal, the PLE spectrum shows no features that could be attributed to excitonic states or processes of electron–hole recombination.

From the energy diagram, Fig. 12 it follows also that the activation energy for thermal quenching of luminescence of the Ce^{3+} impurity center, which is equal to 0.32 eV [4], is due to the non-radiative relaxation from the 5d excited state to the $4f^1$ ground state of Ce^{3+} ion. In other words, there is realized the intracenter thermal quenching of luminescence of Ce^{3+} ions in LGBO:Ce crystals.

4.5. Luminescence of LGBO:Ce upon inner-shell excitation

The luminescence spectra of the crystal LGBO:Ce upon excitation in the energy range of the core transitions consist mainly of the PL emission bands of Gd^{3+} and Ce^{3+} ions. Additional broad luminescence band in the energy range of 3–6 eV is observed in

the PL emission spectrum upon excitation by XUV photons. In the low-energy region, this band is adjacent to the doublet of the Ce^{3+} PL bands, which are due to $5d \rightarrow 4f^1$ transitions from the lowest excited state of the Ce^{3+} ion, and with increasing excitation energy the luminescence intensity gradually decreases to a minimum value at 6 eV. This luminescence can be interpreted as the $5d \rightarrow 4f^1$ radiative transitions from the highly excited 5d states of Ce^{3+} ion. Such transitions were previously observed in YPO_4:Ce^{3+} crystals [49].

The XUV photon absorption in a crystal leads to excitation of one electron onto the CB bottom, and to formation of a hole in the core shell. Core hole relaxes by Auger mechanism, which is realized within the same ion. The Auger cascade process results also in creation of secondary electrons. The absorption coefficient increases significantly in the vicinity of the fundamental absorption edges, which reduces the thickness of the layer in which the radiation is absorbed, and thus increases the surface energy losses. This is also known as the 'giant resonance' [50]. The excitation spectrum in these regions is similar to 'inverted' absorption spectrum. Efficient excitation of intrinsic and extrinsic luminescence bands in the LGBO crystal occurs above the 1 s Li absorption edge at ca. 60 eV. The luminescence intensity increases by approximately 4 times with increasing energy from 60 to 135 eV. Fine structures at Gd 4d fundamental absorption edge (ca. 149 eV) refer to transitions from 4d atomic orbital to the free states in 4f shell. As the 4d orbital is split to $4d_{5/2}$ and $4d_{3/2}$ states by spin-orbital coupling, we can see the same group of lines twice. This behavior is common for all rare earth, the same picture was observed in metals and free ions [51]. A broad dip with a minimum at 148–150 eV is due to the fact that all atoms with a configuration similar to Xe atom exhibit an intense broad peak, the so-called 'giant resonance' in the absorption spectrum, the overall behavior of which depends only slightly on the environment of the absorbing atom [50]. In the energy range of 160–194 eV the PLE spectra are less structured. The total luminescence intensity increases slowly and monotonically with increasing the excitation energy from 160 to 194 eV. The narrow line due to electron transitions from the 1 s B level to the CB bottom of LGBO:Ce crystal is observed at 194.5 eV. A similar picture is observed in the energy range of 1 s oxygen absorption edge, Fig. 10. Note that upon excitation in the energy ranges of 60–135 eV and 145–170 eV the Ce^{3+} emission intensity is much higher than that for Gd^{3+} ion, Fig. 9. Proposed reason for this, in our opinion, is the excitation of core transitions in the Ce^{3+} ions. Indeed, the peak of the giant resonance of cerium is located at ca. 120 eV [50], but the concentration of the cerium impurity in a crystal is much lower than that for the Gd^{3+} host ions. Additional channel of excitation leads to a somewhat higher efficiency of excitation for the Ce^{3+} emission in comparison with that for the intrinsic luminescence of Gd^{3+} ions.

All these features in the PLE spectra are due to an electron transfer from the core level to the CB bottom states. For example, 1 s B line was observed in the PLE spectra at 194.5 eV, Fig. 9. At the same time, the binding energies E_b, determined by an X-ray photoelectron spectroscopy (XPS), are usually presented relative to the Fermi level E_F. From XPS data it follows that the binding energies are 55.6 eV (1 s Li), 189.4 eV (1 s B), 191.4 eV (1 s B in B_2O_3) [52], 192.0 eV (1 s B in LiB_3O_5 crystal) [14,15]. Applying data for boron oxide and lithium triborate crystal, we find that the Fermi level in LGBO:Ce crystal should be located within the bandgap at 2.5–3.1 eV below the CB bottom. With regard to the VB top this amounts 6.2–6.8 eV, and the mean value of $E_F = 6.5$ eV corresponds well with the position of the $4f^{n-1}5d$ levels of the trivalent ions of Ce^{3+} and Gd^{3+} in LGBO:Ce crystal. Refinement of the Fermi level position in LGBO:Ce crystal allows us to compare the calculated values of absolute location of $4f^n$ energy levels E_f in LGBO:Ce, Fig. 13 with the available XPS data because $E_b = E_F - E_f$. Unfortunately, until today the XPS data on LGBO are unavailable.

5. Conclusion

Thus, for the first time we have investigated the UV luminescence of LGBO:Ce crystals with sub-nanosecond time resolution upon selective excitation in the broad energy range from 3.0 to 650 eV at 6–9 and 293 K. The most important results of this work, which were discussed in the light of the available data from literature, are as follows.

1. Intrinsic luminescence of LGBO:Ce crystal, which is manifested as a narrow peak at 3.95–3.97 eV, is due to the $^6P_j \rightarrow {}^8S_{7/2}$ radiative transitions in Gd^{3+} host ions. The luminescence appears at various kinds of excitations: direct photoexcitation of the *f–f* transitions in Gd^{3+} ion, excitation through the charge-transfer transitions (H-band, the CT absorption band O–Gd). The PL intensity is negligible upon excitation at the low-energy tail of the fundamental absorption of a crystal as well as at energies of $(1–3) \times E_g$. Distinguishing features of the luminescence: a remarkably efficient transport of electronic excitation energy along the chains of Gd^{3+} ions at temperatures above 40 K; a weak temperature dependence and the slow decay kinetics due to the weak interaction of 4f-electrons with the external environment.

2. The intrinsic luminescence at 3.95–3.97 eV can be efficiently excited by XUV-photons in the energy ranges of the core transitions in the Li, Gd, B, O host ions. In the energy regions near the 1 s fundamental absorption edge of the lithium, boron, and oxygen atoms as well as in the energy interval of the 'giant resonance' of the $4d \rightarrow 4f$ gadolinium photoionization, the PLE spectrum crucially determined by the absorption spectrum of LGBO crystal.

3. The cerium impurity in LGBO crystal can substitute the Gd^{3+} host ions, which leads to the formation of two types of the luminescence centers Ce1 and Ce2 in the form of a Ce^{3+} ion, which is either associated with a lattice defect, or is located in the defect-free region of the crystal. The broad complex luminescence band in the energy range of 2.0–3.5 eV is a superposition of the PL emission spectra of the Ce1 and Ce2 centers. This PL emission band can be excited both through the direct photoexcitation of the $4f \rightarrow 5d$ transitions in the Ce^{3+} ion, and the transfer of energy from the excited states of Gd^{3+} ions.

4. The impurity related luminescence at 2.0–3.5 eV can be efficiently excited by XUV-photons in the energy ranges of the core transitions in the Li, Gd, B, O host ions. The PL decay kinetics of the impurity related emission of LGBO:Ce crystal exhibits an intensive fast component with the sub-nanosecond lifetime. In addition, there is a new broad band of PL emission, which extends from 3 to 6 eV and caused by the $5d \rightarrow 4f^1$ radiative transitions from the highly excited 5d states of the Ce^{3+} ion.

5. On the basis of the experimental data for LGBO:Ce crystal at 10 K, we have determined the bandgap $E_g = 9.3$ eV, the minimum energy of the $5d \rightarrow 4f^1$ transitions in the Ce^{3+} impurity ion, the minimum energy for the O–Gd charge-transfer transitions, the Fermi level position in LGBO:Ce crystal. The expected energy positions of the 4f and 5d ground states of the divalent and trivalent lanthanide ions in LGBO:Ce crystal were calculated in the model [21,31].

Acknowledgments

The authors are grateful to A.V. Tolmachev and R.P. Yavetskiy for providing the grown crystals for investigation. Many thanks to M. Kirm for his help in conducting the measurements at BW3

beamline. The work was supported partially by HASYLAB DESY, Project No. II-20080019 (SUPERLUMI station, beamline I) and Project No. II-20080199EC (beamline BW3).

References

[1] I.N. Ogorodnikov, V.A. Pustovarov, S.I. Omelkov, A.V. Tolmachev, R.P. Yavetskiy, Opt. Spectrosc. 102 (2007) 60.
[2] C.T. Garapon, B. Jacquier, J.P. Chaminade, C. Fouassier, J. Lumin. 34 (1985) 211.
[3] C.T. Garapon, B. Jacquier, Y. Salem, R. Moncorge, J. de Phys. Colloq. C C7 46 (1985) 141.
[4] I.N. Ogorodnikov, I.N. Sedunova, L.I. Isaenko, S.A. Zhurkov, Phys. Solid State 54 (2012) 485.
[5] I.N. Ogorodnikov, N.E. Poryvai, I.N. Sedunova, A.V. Tolmachev, R.P. Yavetskiy, Opt. Spectrosc. 110 (2011) 266.
[6] E.F. Dolzhenkova, M.F. Dubovik, A.V. Tolmachev, R.P. Yavetskii, Inorg. Mater. 40 (2004) 856.
[7] R.P. Yavetskiy, M. Dubovik, A.V. Tolmachev, V. Tarasov, Phys. Status Solidi. C 2 (2005) 268.
[8] I.N. Ogorodnikov, N.E. Poryvay, V.A. Pustovarov, A.V. Tolmachev, R.P. Yavetskiy, V.Yu. Yakovlev, Radiat. Meas. 45 (2010) 336.
[9] J.B. Czirr, G.M. MacGillivray, R.R. MacGillivray, P.J. Seddon, Nucl. Instrum. Methods Phys. Res. A 424 (1999) 15.
[10] C.W.E. van Eijk, Nucl. Tracks Radiat. Meas. 21 (1993) 5.
[11] A.N. Shekhovtsov, A.V. Tolmachev, M.F. Dubovik, E.F. Dolzhenkova, T.I. Korshikova, B.V. Grinyov, V.N. Baumer, O.V. Zelenskaya, J. Cryst. Growth 242 (2002) 167.
[12] G. Zimmerer, Radiat. Meas. 42 (2007) 859.
[13] R.T. Wegh, A. Meijerink, R.J. Lamminmäki, J. Hölsä, J. Lumin. 87–89 (2000) 1002.
[14] A.Yu. Kuznetsov, M.V. Kuznetsov, I.N. Ogorodnikov, A.V. Kruzhalov, V.A. Maslov, Phys. Solid State 36 (1994) 465.
[15] I.N. Ogorodnikov, V.A. Pustovarov, M. Kirm, Phys. Solid State 46 (2004) 842.
[16] A.Yu. Kuznetsov, A.V. Kruzhalov, I.N. Ogorodnikov, A.B. Sobolev, L.I. Isaenko, Phys. Solid State 41 (1999) 48.
[17] I.N. Ogorodnikov, V.A. Pustovarov, A.V. Kruzhalov, L.I. Isaenko, M. Kirm, G. Zimmerer, Phys. Solid State 42 (2000) 464.
[18] Y.N. Xu, W.Y. Ching, R.H. French, Phys. Rev. B: Cond. Matter 48 (1993) 17695.
[19] Y. Wang, X. Guo, T. Endo, Y. Murakami, M. Ushirozawa, J. Solid State Chem. 177 (2004) 2242.
[20] F. Shen, D. He, H. Liu, J. Xu, J. Lumin. 122–123 (2007) 973.
[21] P. Dorenbos, J. Lumin. 111 (2005) 89.
[22] K.C. Mishra, B.G. De Boer, P.C. Schmidt, I. Osterloh, M. Stephan, V. Eyert, K.H. Johnson, Ber. der Bunsen Phys. Chem. Chem. Phys. 102 (1998) 1772.
[23] J.F. Rivas-Silva, A. Flores-Riveros, M. Berrondo, Int. J. Quantum Chem. 94 (2003) 105.
[24] V.N. Abramov, A.N. Ermoshkin, A.I. Kuznetsov, V.V. Mürk, Phys. Status Solidi B 121 (1984) K59.
[25] A. Lushchik, M. Kirm, Ch. Lushchik, I. Martinson, G. Zimmerer, J. Lumin. 87–89 (2000) 232.
[26] V. Kisand, R. Kink, M. Kink, J. Maksimov, M. Kirm, I. Martinson, Phys. Scr. 54 (1996) 542.
[27] I.V. Kityk, A. Mefleh, Physica B 262 (1999) 170.
[28] A.J. Nelson, J.J. Adams, K.I. Schaffers, Appl. Surf. Sci. 252 (2005) 1228.
[29] G.H. Dieke, Spectra and Energy Levels of Rare Earth Ions in Crystals, Wiley Interscience, New York, 1968.
[30] P. Dorenbos, J. Lumin. 122–123 (2007) 315.
[31] P. Dorenbos, J. Lumin. 91 (2000) 155.
[32] C.K. Jørgensen, Prog. Inorg. Chem. 12 (1970) 101.
[33] P.A. Rodny, I.V. Khodyuk, G.B. Stryganyuk, Phys. Solid State 50 (2008) 1639.
[34] A.N. Belsky, J.C. Krupa, Displays 19 (1999) 185.
[35] X. Wu, H. You, H. Cui, X. Zen, G. Hong, C.H. Kim, C.H. Pyun, B.Y. Yu, C.H. Park, Mater. Res. Bull. 37 (2002) 1531.
[36] Ch. Pédrini, Phys. Status Solidi A 202 (2005) 185.
[37] M. Leskelä, J. Hölsä, Eur. J. Solid State Inorg. Chem. 28 (1991) 151.
[38] R.S. Eachus, M.C.R. Symons, J. Chem. Soc. A (1968) 2438.
[39] B. Han, H.B. Liang, H.H. Lin, J.P. Zhong, Q. Su, P. Dorenbos, M.D. Birowosuto, G.B. Zhang, Y.B. Fu, J. Appl. Phys. 101 (2007) 113530(8).
[40] O.A. Anikeenok, Phys. Solid State 48 (2006) 1878.
[41] E. Nakazawa, J. Lumin. 100 (2002) 89.
[42] D. Hou, B. Han, W. Chen, H. Liang, Q. Su, P. Dorenbos, Y. Huang, Z. Gao, Y. Tao, J. Appl. Phys. 108 (2010) 083527(6).
[43] F. Yang, S.K. Pan, D.Z. Ding, X.F. Chen, S. Lu, W.D. Zhang, G.H. Ren, J. Alloys Compd. 484 (2009) 837.
[44] C.W. Thiel, H. Cruguel, Y. Sun, G.J. Lapeyre, R.M. Macfarlane, R.W. Equall, R.L. Cone, J. Lumin. 94–95 (2001) 1.
[45] C.W. Thiel, H. Cruguel, H. Wu, Y. Sun, G.J. Lapeyre, R.L. Cone, R.W. Equall, R.M. Macfarlane, Phys. Rev. B 64 (2001) 085107(13).
[46] M. Kirm, A. Lushchik. Ch. Lushchik, G. Zimmerer, in: Physics and Chemistry of Luminescent Materials, PV 99–40, The Electrochemical Society Proceeding Series, Pennington, NJ, 2000, pp. 113–122.
[47] Ch. Pédrini, L. Zhang, C. Dujardin, A. Petrosyan, A.N. Belsky, Radiat. Eff. Defect Solid 150 (1999) 29.
[48] P. Dorenbos, E.V.D. van Loef, C.W.E. van Eijk, K.W. Krämer, H.U. Güdel, Phys. Rev. B: Cond. Matter 68 (2003) 125108(6).
[49] N.P. Karanjikar, R.C. Naik, Solid State Commun. 65 (1988) 1419.
[50] T.M. Zimkina, V.A. Fomichev, S.A. Gribovsky, I.I. Zhukova, Sov. Phys. Solid State 9 (1967) 1128.
[51] C.D. Olson, D.W. Lynch, J. Opt. Soc. Am. 72 (1982) 88.
[52] V.I. Nefedov, Handbook of X-Ray Photoelectron Spectroscopy of Chemical Compounds, Khimiya, Moscow, 1984. (in Russian).
[53] L. Tian, B.Y. Yu, C.H. Pyun, H.L. Park, S.I. Mho, Solid State Commun. 129 (2004) 43.
[54] H.C. Yang, C.Y. Li, H. He, Y. Tao, J. Xu, Q. Su, J. Lumin. 118 (2006) 61.
[55] Z. Wang, Y. Wang, J. Zhang, J. Rare Earths 26 (2008) 425.
[56] Y.H. Wang, K. Uheda, H. Takizawa, U. Mizumoto, T. Endo, J. Electrochem. Soc. 148 (2001) G430.
[57] Y.H. Wang, X.X. Li, J. Electrochem. Soc. 153 (2006) G238.